

Spatial distributions of Balmer series emissions in divertor plasmas with tungsten targets in different magnetic configurations on the EAST superconducting tokamak

Kunpei Nojiri (野尻訓平)¹, Naoko Ashikawa (芦川直子)^{2,3}, Yasuhiro Suzuki (鈴木康浩)^{2,3}, Yaowei Yu (余耀伟)⁴, Zhenhua Hu (胡振华)⁴, Fang Ding (丁芳)⁴, Liang Wang (王亮)⁴, Lingyi Meng (孟令义)⁴, Xiahua Chen (陈夏华)⁴, Jie Huang (黄杰)², Zhongshi Yang (杨钟时)⁴, Tetsutaro Oishi (大石鉄太郎)^{2,3}, Mizuki Sakamoto (坂本瑞樹)¹, Jiansheng Hu (胡建生)⁴, Guangnan Luo (罗广南)⁴

¹Plasma Research Center, University of Tsukuba, 1-1-1 Tennodai, Tsukuba 305-8577, Japan

²National Institute for Fusion Science, National Institutes of Natural Sciences, Oroshi-cho, 322-6, Toki 509-5292, Japan

³Department of Fusion Science, Graduate University for Advanced Studies, SOKENDAI, Oroshi-cho, 322-6, Toki 509-5292, Japan

⁴Institute of Plasma Physics, Chinese Academy of Sciences, Hefei 230031, People's Republic of China

E-mail: nojiri_kunpei@prc.tsukuba.ac.jp

Received xxxxxx

Accepted for publication xxxxxx

Published xxxxxx

Abstract

The characteristics of wall recycling with different divertor configurations were investigated in this study, focusing on the observations of the spatial distributions of deuterium atomic emissions in the Balmer series (D_α , D_β , D_γ , and D_δ) with different magnetic field configurations in the Experimental Advanced Superconducting Tokamak. The observed D_α and D_β emissions were primarily relatively close to the divertor targets, while the D_γ and D_δ emissions were primarily relatively close to the X-point. The distributions of the emissions close to the divertor targets and X-point changed differently depending on the divertor configuration. These experimental results indicate that the linear comparison of parameters based on an assumption of similarity of profile shapes in different configurations is insufficient for understanding particle recycling in divertor plasmas. This is because the shape of the density profile of the recycled deuterium atoms and/or the electron density and temperature may change when the magnetic configuration is altered.

Keywords: deuterium recycling, tungsten divertor, strike point position, deuterium atomic emissions

1. Introduction

Hydrogen isotope recycling at divertor targets plays important roles in core plasma performance [1–3]. Injected fuel particles (hydrogen isotopes) are ionized, and some of the fuel ions eventually reach walls. After reaching the walls, the ions are reflected as neutral atoms or absorbed by the walls.

Some of the absorbed ions are re-emitted in the form of neutral molecules. These recycled neutral atoms and molecules may re-enter the plasma and cause interactions such as refueling [4]. Recycling control will be even more important in future fusion devices with long-pulse operation, such as ITER [5, 6] and DEMO [7, 8], to maintain core plasma performance. The material species of the walls is an important factor in

determining the recycling characteristics [9]. ITER will use tungsten (W) as the divertor material, which is also a candidate material for DEMO. The recycling characteristics additionally depend on wall conditions such as retention, temperature, and deposition [10]; the divertor geometry and configuration [2, 11]; and plasma parameters. Since these effects on recycling change with the position in the divertor region, it is necessary to investigate the parameters related to recycling at various positions. Thus, it is important to assess the spatial effects of the divertor configuration on the recycling characteristics with W divertor plates.

For recycling studies in tokamaks, hydrogen isotope atomic emissions, especially Balmer series emissions such as D_α and D_β , are widely used. Some of the neutral atoms generated by reflection at the walls and dissociation of the re-emitted molecules from the walls are excited by electrons, and Balmer series emissions are observed. Thus, atomic emissions are effective monitors of recycling neutrals. These observed emissions are often the results of integration along the lines of sight (LOSs) of spectrometer systems, meaning that there is uncertainty in the locations of the recycled atoms. To evaluate local emissions, techniques such as tomography [12] and Zeeman patterns in spectral shapes [13] are used. Meanwhile, for emissions from higher excited states such as D_γ and D_δ , their ratios to D_α are widely utilized as indicators of volumetric recombination [14]. In contrast, in ionizing plasma, the ratio becomes larger with decreasing electron density n_e [15], while its dependence on the electron temperature T_e is relatively small. In the scrape-off layer (SOL)/divertor region, since n_e changes significantly with position, the spatial distributions of the different Balmer series emissions in ionizing plasma can be compared to estimate the locations of emissions from recycled atoms. This method is simple and involves relatively basic spectroscopic system setups. Therefore, observations of the spatial distributions of Balmer series emissions with different configurations are effective for elucidating the spatial effects of the divertor configuration on the recycling characteristics.

In the Experimental Advanced Superconducting Tokamak (EAST), a water-cooled W monoblock is used for the upper divertor [16]. Recently, utilizing superconducting coils, heating systems and feedback control systems, H-mode operation over 100 s has been achieved with an upper single-null (USN) configuration [16–18]. Meanwhile, it has been observed that the strike point (SP) positions at the W divertor (configuration) alter the exhaust efficiency of the recycled neutrals, which is a spatially averaged characteristic of recycling, focusing on the density decay of the bulk plasma after gas puffing is stopped [18, 19]. To elucidate the spatial effects of the divertor configuration on the recycling characteristics with a W divertor, the spatial distributions of Balmer series emissions in the divertor region with different configurations were investigated in this study.

2. Experimental setup

Deuterium plasma discharge is conducted with a USN divertor configuration in EAST. The upper divertor is equipped with water-cooled W/Cu plasma-facing components [16]. An in-vessel cryopump is installed for particle exhaust through a vacuum pumping slot at the corner of the upper outer (UO) divertor region, as shown in figure 1(a). The exhaust pressure is measured by a cold cathode ionization gauge.

Multichannel spectroscopic systems of the deuterium Balmer series (D_α , D_β , D_γ , and D_δ) are installed. Figure 1(a) shows the LOSs mapped to a poloidal cross-section. The LOSs of the system start from an optical vacuum window located below the equatorial plane and extend to UO divertor targets at different toroidal positions. Three sets of optical fiber systems are used: D_α , D_β , and D_γ and D_δ . Hence, different LOSs are shown in figure 1(b). The obtained counts in the spectroscopy systems are integrated values along the relatively complicated LOSs. However, it is considered that emissions from neutral deuterium atoms are mainly produced between the X-point and UO divertor targets. The system for D_α measurement included a photomultiplier tube; the D_γ and D_δ emissions were measured by a spectrometer with an electron-multiplying charge coupled device (EMCCD) [20]; and an additional multichannel spectrometer system with an EMCCD was used for the D_β measurements. Relative intensity calibration of the D_γ and D_δ measurements was performed previously to obtain their spatial distributions. For the D_α and D_β measurements, precise relative calibration has not been conducted, but these signal intensities were adjusted to reduce differences in sensitivity among the observation channels. On the UO divertor targets, 13 Langmuir probes (LPs) are installed in one poloidal section [21], as shown in figure 1(b), and those at port O were used in this study. Data acquisition of the LPs and D_α was conducted about every 0.02 ms and 0.01 ms, respectively. The exposure times for the D_β measurements and the D_γ and D_δ measurements were 5 ms and 10 ms, respectively, and sampling rates were about 100 Hz.

3. Experimental results and discussion

The plasma experiment was performed with the USN configuration, a toroidal magnetic field B_T of ~ 2.4 T (normal field), a plasma current I_p of ~ 400 kA, and lower hybrid wave heating with a power of ~ 1 MW in L-mode (shot # 93922).

For plasma operation with different divertor magnetic configurations under similar background conditions of plasma-facing walls, the SP was swept at the UO divertor. The line-averaged density \bar{n}_e was set to $\sim 3 \times 10^{19} \text{ m}^{-3}$ by a density feedback control via supersonic molecular beam injection. As shown in figure 2, I_p and \bar{n}_e were kept almost constant from time $t = 3.3$ s to 6.3 s, and the SP position calculated by EFIT was shifted from a distance from the UO divertor corner d of 8 cm to 12 cm along the divertor targets. Thus, the divertor SP moved away from the vacuum pumping slot.

From $t \approx 3.4$ s to 5.0 s, the divertor neutral pressure $P_{n,\text{div}}$ decreased, which is consistent with the experimental results on

particle exhaust efficiency optimization regarding the SP position at the divertor targets [18, 19]. However, from $t \approx 5.0$ s to 6.5 s, although the SP position continued moving away from the slot, $P_{n,div}$ increased. This finding is different from the results published in the abovementioned literature, where the SP was located at $d = 5-8$ cm. Based on this difference, it was assumed that the neutral pressures do not simply depend on the SP position from the vacuum pumping slot. Hence, additional investigations of other effects on $P_{n,div}$ are required.

In this study, the SP position was confirmed by experimental data obtained by LPs on divertor targets in addition to numerical calculations performed using EFIT. Figure 3 shows the separatrixes calculated by EFIT at $t = 3.3, 3.6, 4.8, 5.4,$ and 6.3 s at plasma discharge #93922. At $t = 3.3, 3.6, 4.8, 5.4,$ and 6.3 s, $d = 8, 9, 10, 11,$ and 12 cm, respectively. When the SP position shifts from the inner to outer side, the position of the X-point also moves radially outward.

Figure 4(a) shows the time evolution of the spatial distribution of the ion saturation current I_s measured by LPs on divertor targets. Figures 4(b) and (c) present the spectroscopy data of D_γ and D_δ as spatial distributions projected onto divertor targets. I_s in figure 4(a) was obtained using values averaged over every 10 ms, and the intensities of D_γ and D_δ acquired in one exposure time (10 ms) are plotted in figures 4(b) and (c), respectively. This time is sufficiently short to follow the change in SP position. When the SP moves from $d = 8$ cm to 12 cm, the peak positions of I_s , D_γ , and D_δ also move outward. Some of the peak positions of I_s almost exactly match the SP positions. On the other hand, the positions corresponding to higher intensities of D_γ and D_δ occur more than 2 cm outside the SP according to the projected positions on the divertor targets. This LOS with the peak intensities of D_γ and D_δ passes above the X-point, as shown in figure 1(b).

Figure 5 presents the time evolution of the intensities of D_α and D_β measured by multichannel spectroscopy. The positions, as shown from 6.1 cm to 20.7 cm, are the projected positions of the integrated signals along the LOSs to the divertor targets, as depicted in figure 1(b). The intensities of D_α averaged over every 2 ms and the intensities of D_β corresponding to every 5 ms exposure are plotted. When the SP position is around 8 cm, higher intensities of D_α and D_β are observable at the projected position of 10 cm. This tendency is similar to that of the peaks of I_s around the SP position of 8 cm in figure 4(a). After that, with outward movement of the SP, the intensities of D_α and D_β at the projected positions of 10 cm and 12 cm decrease. On the other hand, when the SP moves from 10 cm to 12 cm, the intensities at the projected positions of 15–21 cm increase. Thus, with an SP position of 12 cm, the projected positions of higher intensities of D_α and D_β seem to be located in the range of 15–21 cm. These findings also suggest that the projected position of higher intensity moves 5–11 cm outward when the SP moves from $d = 8$ cm to 12 cm.

Figure 6(a) shows the spatial distributions of I_s on the divertor targets. Figures 6(b) and (c) present the projected

spatial distributions of D_γ and D_δ with SP positions of $d = 8, 9, 10, 11,$ and 12 cm ($t = 3.3, 3.6, 4.8, 5.4,$ and 6.3 s). Figure 6 plots the values averaged over every 100 ms and provides the details of the spatial distributions. When $d = 8, 10,$ and 12 cm, the peak positions of I_s are shifted up to 1 cm from the SP position, including consideration of the spatial resolution error due to the limited number of LPs. Further, I_s peaks are not observable near the SP position when $d = 9$ and 11 cm. Judging from the SP position, the peak positions of I_s are considered to be in the range from 7 cm to 14 cm, and I_s positions greater than 14 cm are not considered to be peaks.

In the projected spatial distributions of D_γ and D_δ on the divertor targets, peak positions occur at 13–17 cm when the SP position is 8–12 cm, and the projected peak positions are about 4 cm outward from the SP position. The projected spatial distribution of D_γ shows a widely expanded tail on the inward side when the SP is at $d = 8$ cm, but the D_γ distributions when the SP is at $d = 12$ cm do not have such larger tails below 12 cm. Therefore, the D_γ intensities for the two SPs, which correspond to different magnetic configurations, suggest different spatial profile shapes. The difference between the positions of the maximum intensities on the divertor targets in the cases in which the SP is located at $d = 8$ and 12 cm is about 2 cm. The signal-to-noise ratio of the D_δ intensity is low due to the low count of D_δ , whose maximum count is only about 30; thus, the errors for the peak positions are greater than those for the D_γ peaks. However, the peak position of D_δ in the case in which the SP is located at $d = 8$ cm is at least inside the peak position corresponding to $d = 12$ cm, and the peak positions differ by up to 4 cm. Note that the spatial profile shapes of D_γ and D_δ are significantly different from that of I_s . I_s is related to the local product of n_e and the ion sound speed at the divertor plate. On the other hand, the intensities of D_γ and D_δ are related to the integrated values of the local product of n_e , the deuterium atomic density, and the rate coefficients of the excitation reactions along the entire LOS, including the divertor plates and X-point. The analyses of the profile shape differences with these parameters taken into account are planned.

As discussed in relation to figure 5, the projected positions of higher intensities of D_α and D_β are around 10 cm and in the range of 15–21 cm when the SP is located at $d = 8$ and 12 cm, respectively. The peak positions of the projected D_γ and D_δ intensities in figures 6(b) and (c) are around 13 and 17 cm when the SP is located at $d = 8$ and 12 cm, respectively. All the projected positions of the deuterium atomic emissions are outside the SP positions. Following the LOSs in figure 1(b), it can be understood that as the projected position becomes more distant, the LOS crosses a point further upstream in the separatrix. If the emissions of deuterium atoms are released along divertor magnetic field lines from the X-point to the divertor targets, the emissions between the X-point and the vicinity of the divertor targets are dominant, rather than those in the vicinity of the divertor targets. In addition, when the SP is located at $d = 8$ cm, the projected positions of the D_γ and D_δ

peaks are farther away than those of higher D_α and D_β intensities. This finding suggests that D_γ and D_δ emissions are dominant on the X-point side of the above region, while D_α and D_β emissions are dominant on the divertor side. In ionizing plasma, intensity ratios such as D_γ/D_β and D_δ/D_β considerably decrease with n_e and moderately increase with T_e in the n_e range of 10^{16} – 10^{20} m⁻³ [15]. In the SOL/divertor region of EAST, n_e has generally been observed to be within this range [21, 22]. In this experiment, it is considered that n_e decreased and T_e increased from the divertor targets to the X-point. Therefore, it can be considered that higher D_α and D_β emissions occurred relatively close to the divertor targets, while those of D_γ and D_δ occurred relatively close to the X-point. It should be noted that the projected positions of higher D_α and D_β intensities moved by at least 5 cm and those of D_γ and D_δ moved by up to 4 cm. This difference indicates that the distributions of the strong emissions near the divertor targets and those near the X-point change differently depending on the magnetic field configuration. It can be also understood that the change in the profile shape of D_γ means that the profile shape of the emission near the X-point changes with the configuration. These results suggest that the distribution of the density of recycled deuterium atoms and/or n_e and T_e changed, since the emission intensities are functions of the atomic density n_e and a rate coefficient of excitation that depends on T_e . Therefore, to understand the spatial distribution of the density of recycled atoms, it is necessary to evaluate local emissions using experimental data, i.e., three-dimensional LOS and magnetic field data, and numerical simulation data for the edge plasma.

In EAST, wall recycling has been investigated in relation to the vacuum pumping efficiency, effects of Li coating, and plasma-facing materials. In the present study, the spatial distributions of deuterium atomic emissions in the edge plasma regions were observed, and the characteristics of the distributions corresponding to different magnetic configurations were identified. The spatial profile shapes of the density of recycled atoms and/or n_e and T_e could change when the magnetic configuration changed. Consequently, linear comparison of parameters with different configurations assuming similarity of profile shapes is insufficient. Future devices such as the China Fusion Engineering Test Reactor [23] and ITER have large plasma-facing areas and their operations are planned to be long-pulse, and wall recycling control remains an important issue for density control. Therefore, it is important to clarify the spatial behaviors of the local emissions related to wall recycling during plasma experiments to achieve density control during steady-state operations, as shown in this study.

4. Conclusions

This paper focused on the spatial effects of the divertor configuration on the recycling characteristics in the W divertor region. So far in EAST, it has been confirmed that the

configuration changes the exhaust efficiency of the recycled neutrals throughout the W divertor region, which is a spatially averaged characteristic. In this study, the spatial distributions of deuterium atomic emissions in edge plasma regions were observed, and the characteristics of their spatial distributions with different magnetic configurations were identified. Based on the observations, the differences among the D_α , D_β , D_γ , and D_δ distributions were determined, and it can be considered that the distributions of the density of recycled deuterium atoms and/or n_e and T_e change with the magnetic configuration. In particular, D_α and D_β emissions are dominant relatively close to the divertor targets, while D_γ and D_δ emissions are dominant relatively close to the X-point region rather than close to the divertor targets. The distributions of the emissions from deuterium atoms relatively close to the divertor targets and X-point change differently with the magnetic field configuration. The shape of the emission profile near the X-point also changes clearly. These experimental results indicate that linear comparison of parameters assuming similarity of profile shapes with different configurations is insufficient, because the spatial profile shapes of the density of recycled atoms and/or n_e and T_e may change depending on the configuration.

In the future, it is planned to compare the experimental results with numerical simulation results for edge plasma parameters using three-dimensional LOS and magnetic field data to evaluate local deuterium atom emissions and to improve understanding of the spatial distribution of the density of recycled deuterium atoms.

Acknowledgments

This work is supported by JSPS-CAS Bilateral Joint Research Projects, “Control of wall recycling on metallic plasma facing materials in fusion reactor,” 2019-2022, (GJHZ201984 and JPJSBP120197202).

References

- [1] McCormick K *et al* 1990 *J. Nucl. Mater.* **176&177** 89
- [2] Tamain P *et al* 2015 *J. Nucl. Mater.* **463** 450
- [3] Kugel H W *et al* 2009 *J. Nucl. Mater.* **390** 1000
- [4] Sakamoto M *et al* 2004 *Nucl. Fusion* **44** 693
- [5] Aymar R *et al* 2002 *Plasma Phys. Control. Fusion* **44** 519
- [6] Pitts R A *et al* 2019 *Nucl. Mater. Energy* **20** 100696
- [7] Federici G *et al.* 2016 *Fusion Eng. Des.* **109–111** 1464
- [8] Tobita K *et al* 2018 *Fusion Eng. Des.* **136** 1024
- [9] Wissen S *et al* 2017 *Nucl. Fusion* **57** 066024
- [10] de la Cal E *et al* 2020 *Plasma Phys. Control. Fusion* **66** 035006
- [11] Loarte A *et al* 2001 *Plasma Phys. Control. Fusion* **43** R183
- [12] Fujimoto K *et al* 2007 *Trans. Fusion Sci. Tec.* **51** 247
- [13] Shikama T *et al* 2006 *Plasma Phys. Control. Fusion* **48** 1125
- [14] McCracken G M *et al* 1998 *Nucl. Fusion* **38** 619
- [15] Fujimoto T *et al* 1988 *Nucl. Fusion* **28** 1255

- [16] Gong X *et al* 2019 *Nucl. Fusion* **59** 086030
- [17] Wan B N *et al* 2019 *Nucl. Fusion* **59** 112003
- [18] Wang L *et al* 2019 *Nucl. Fusion* **59** 086036
- [19] Liu H *et al* 2017 *Plasma Sci. Technol.* **19** 095101
- [20] Mao H *et al.* 2017 *Rev. Sci. Instrum.* **88** 043502
- [21] Xu J C *et al.* 2016 *Rev. Sci. Instrum.* **87** 083504
- [22] Zhang W *et al.* 2010 *Rev. Sci. Instrum.* **81** 113501
- [23] Wan Y *et al* 2017 *Nucl. Fusion* **57** 102009

Figures

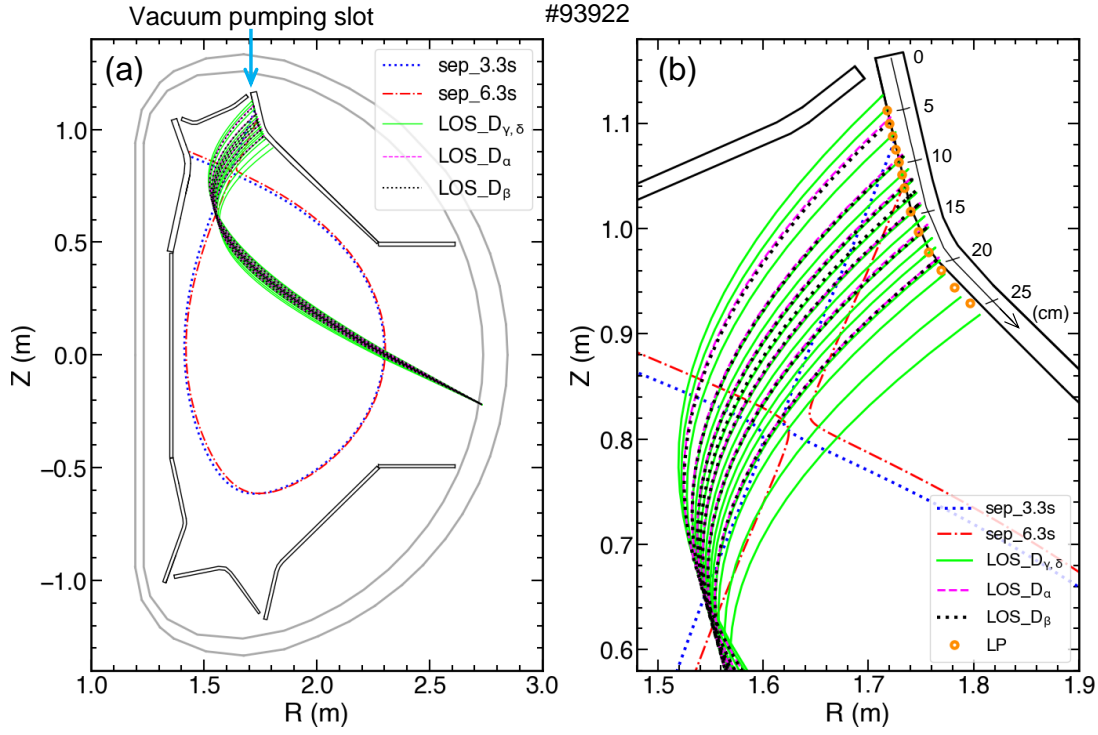


Figure 1. (a) Poloidal cross-section of EAST with separatrices and LOSs mapped onto the poloidal plane, which are adopted by the multichannel visible spectroscopy systems for deuterium Balmer series measurements in the upper W divertor. (b) Enlarged view of the divertor region with the positions of the LPs on the divertor targets. Both graphs show two kinds of separatrices obtained by EFIT at different times, $t = 3.3$ and 6.3 s, in #93922.

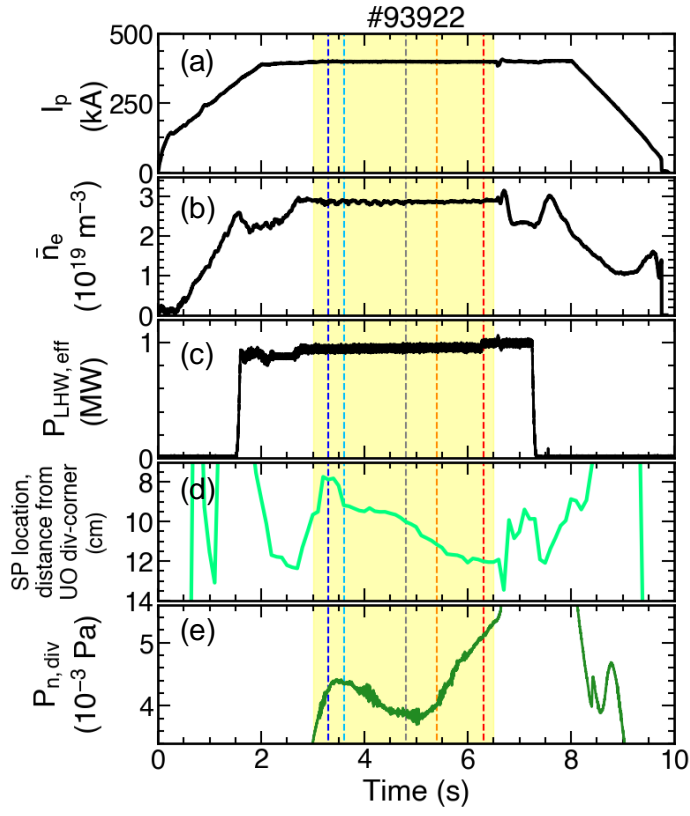


Figure 2. Time evolution of (a) I_p , (b) \bar{n}_e , (c) effective (injected - reflected) power of lower hybrid wave, (d) SP position as described by d , and (e) $P_{n, \text{div}}$.

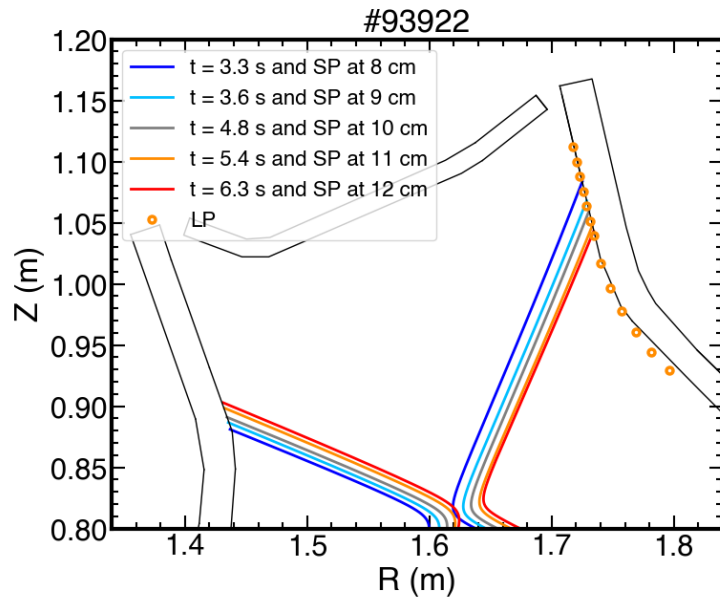


Figure 3. Separatrices around the divertor region at each selected time in #93922 and positions of LPs on the UO divertor with the SP.

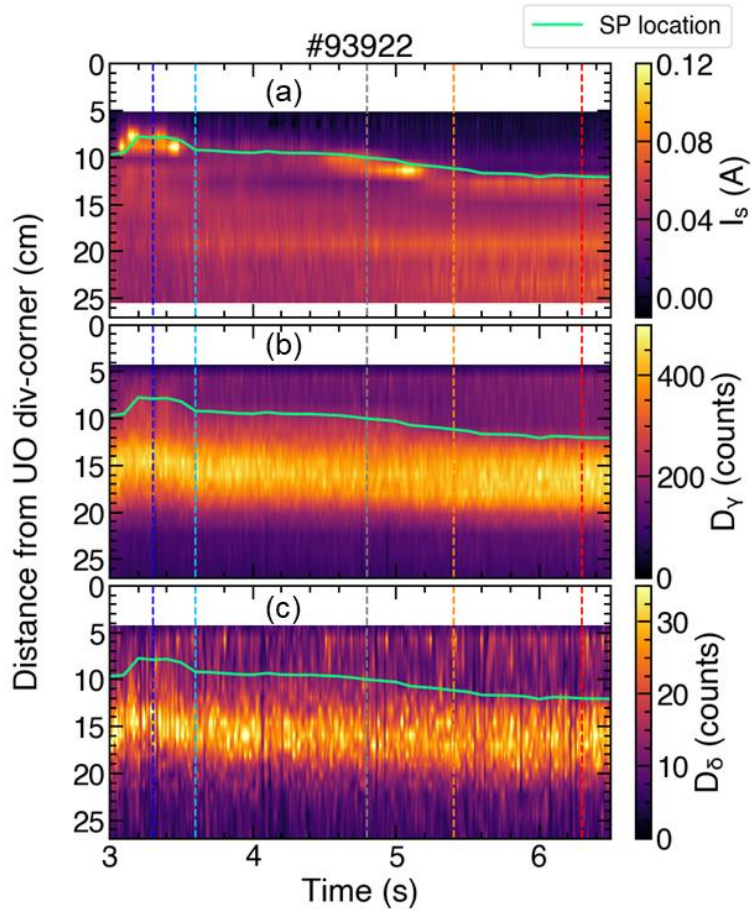


Figure 4. (a) Time evolution of the spatial distribution of I_s on the UO divertor. Projected spatial distributions of (b) D_γ and (c) D_δ intensities on the divertor targets. The green line shows the position of the divertor SP on the UO divertor as described by d .

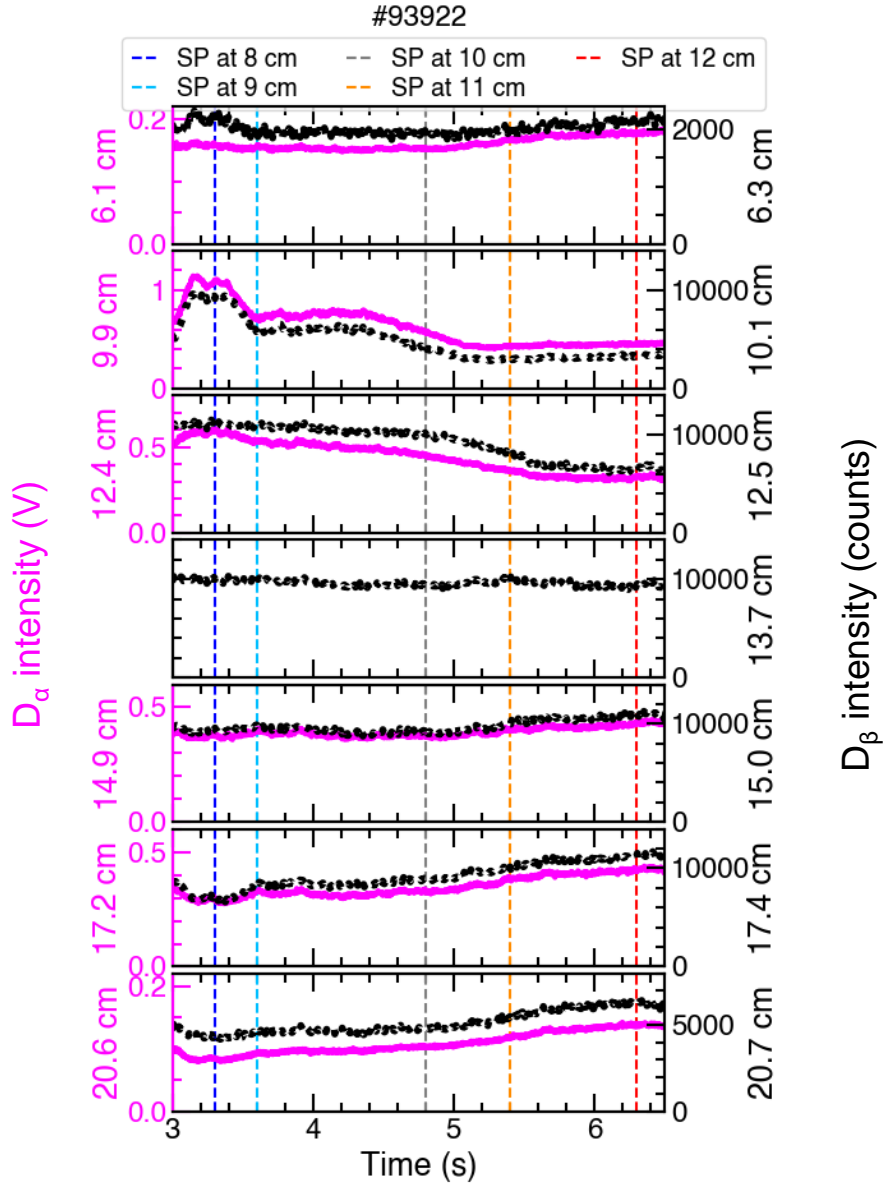


Figure 5. Time evolution of D_α (left) and D_β (right) intensities measured by multichannel spectroscopy. Each position, as shown from 6.1 cm to 21 cm, is the projected position of an LOS to the divertor targets.

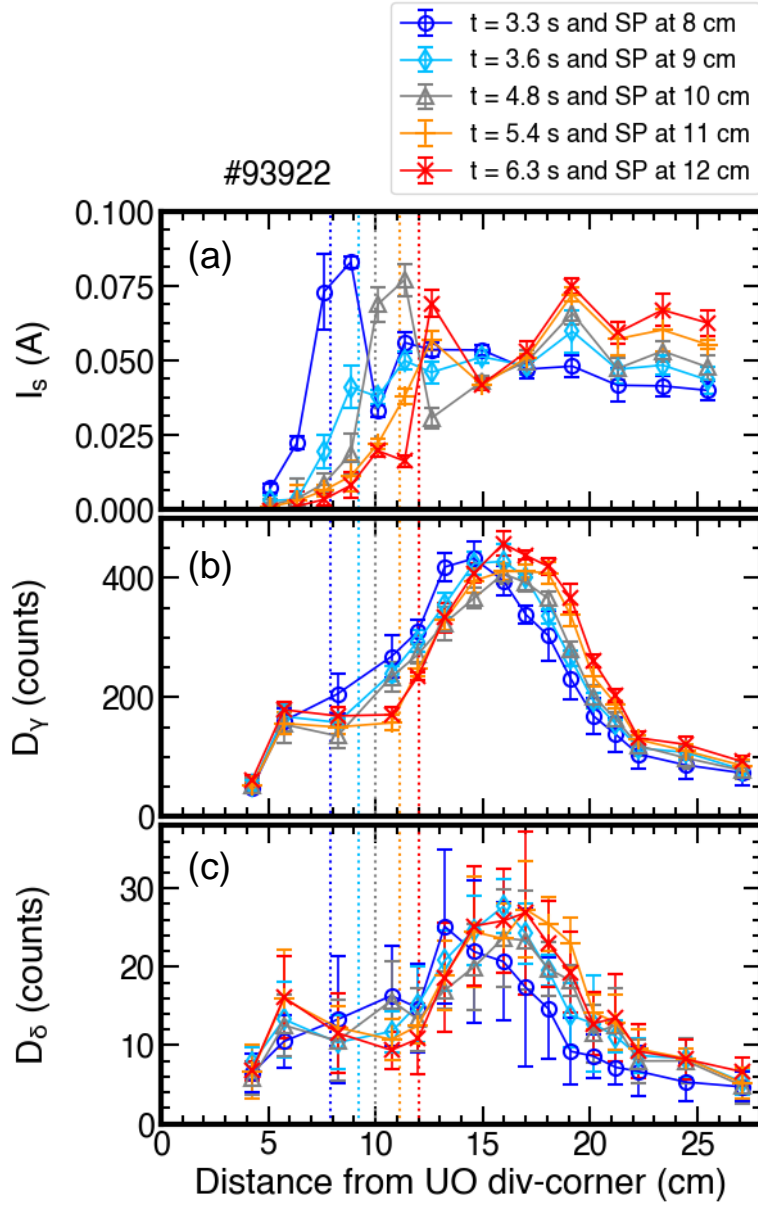


Figure 6. (a) Spatial distributions of I_s on divertor targets. Projected spatial distributions of (b) D_γ , and (c) D_δ intensities on the UO divertor at each selected time. The dashed lines show the positions of the divertor SP on the UO divertor as described by d .